Published in final edited form as:
Biochim Biophys Acta. 2011 January ; 1808(1): 415–423. doi:10.1016/j.bbamem.2010.09.014.

Conformational Plasticity of the Influenza A M2 Transmembrane Helix in Lipid Bilayers Under Varying pH, Drug Binding and Membrane Thickness

Fanghao Hu, **Wenbin Luo**[1], **Sarah D. Cady**, and **Mei Hong**[*]
Department of Chemistry, Iowa State University, Ames, IA 50011

Abstract

Membrane proteins change their conformations to respond to environmental cues, thus conformational plasticity is important for function. The influenza A M2 protein forms an acid-activated proton channel important for the virus lifecycle. Here we have used solid-state NMR spectroscopy to examine the conformational plasticity of membrane-bound transmembrane domain of M2 (M2TM). ^{13}C and ^{15}N chemical shifts indicate coupled conformational changes of several pore-facing residues due to changes in bilayer thickness, drug binding and pH. The structural changes are attributed to the formation of a well-defined helical kink at G34 in the drug-bound state and in thick lipid bilayers, non-ideal backbone conformation of the secondary-gate residue V27 in the presence of drug, and non-ideal conformation of the proton-sensing residue H37 at high pH. The chemical shifts constrained the (ϕ, ψ) torsion angles for three basis states, the equilibrium among which explains the multiple resonances per site in the NMR spectra under different combinations of bilayer thickness, drug binding and pH conditions. Thus, conformational plasticity is important for the proton conduction and inhibition of M2TM. The study illustrates the utility of NMR chemical shifts for probing the structural plasticity and folding of membrane proteins.

Keywords

conformational changes; influenza virus; M2 proton channel; amantadine; membrane thickness; solid-state NMR

Introduction

Membrane proteins carry out their functions by changing their structures under specific environmental cues. They can switch between active and inactive functional states by ion concentration changes [1], ligand binding [2], exposure to hydrophobic lipid bilayers [3-5], and changes in mechanical pressure [6,7]. Oligomeric membrane proteins are particularly malleable to environmental influences [8], since the monomers are held together by weak

Corresponding author: Mei Hong, Tel: 515-294-3521, Fax: 515-294-0105, mhong@iastate.edu.
[1]Current address: 10 Chemistry Building, Penn State NMR Facility, Department of Chemistry, Penn State University, University Park, PA 16802

non-covalent interactions that are susceptible not only to chemical changes but also to physical changes such as the membrane fluidity and thickness. An increasing body of literature suggests that oligomeric membrane proteins may be predisposed to conformational changes by significant conformational distributions due to a rough potential energy surface [9,10].

The M2 protein of influenza A viruses presents a particularly interesting and complex example of how membrane protein conformations depend on the environment. The M2 protein forms a pH-gated tetrameric proton channel in the virus envelope that is important for virus replication [11,12]. Opened by acidic pH of the endosome that encapsulates the virus after its endocytosis, the M2 protein initiates the release of the viral ribonucleoprotein complex into the host cell. The M2 protein is inhibited by the antiviral drug amantadine at a stoichiometric ratio of one drug per channel [13]. The membrane-spanning helix of the M2 protein contains the pH-sensing [14], gating [15], and amantadine-binding residues [16], and is thus the functional core of the protein [17]. High-resolution structures of the M2 transmembrane domain (M2TM) complexed with amantadine have been determined at low pH using X-ray crystallography [18] and at high pH by solid-state NMR [16]. The structure of a longer construct of the M2 protein containing the transmembrane domain was also reported [19]. While these structures gave rich insights into the inhibition and proton conduction mechanisms of M2, they represent only snapshots of the protein structure under the specific conditions of the experiments and do not fully capture the conformational changes and plasticity of the protein. Indeed, significant variations among the three structures exist: for example, the helix orientations and the sidechain conformations of the essential proton-selective and channel-gating residues differed, suggesting the environmental dependence of M2TM structure.

The conformational plasticity of membrane-bound M2TM under a range of experimental conditions has been documented by Cross and coworkers based on ^{15}N solid-state NMR (SSNMR) experiments on oriented membranes [20]. These static ^{15}N NMR spectra report the peptide orientation relative to the bilayer normal, thus frequency and linewidth changes indicate changes of the helix orientations and orientation distribution. It was found that solvents used to reconstitute M2TM into lipid bilayers, amantadine, and pH all affected the helix orientation [20]. Complementarily, magic-angle-spinning (MAS) ^{13}C and ^{15}N NMR spectra [21,22] are sensitive to both the backbone conformation and the helix orientation. MAS spectra of M2TM in unoriented liposomes showed that the helix orientation was influenced by the membrane thickness [23], consistent with EPR results [24]. Moreover, the helical bundle dynamics was found to be extremely sensitive to the membrane composition and fluidity [22]. In addition, the stability of M2TM tetramers in detergent micelles and lipid bilayers have been extensively characterized using analytical ultracentrifugation experiments [25,26].

The purpose of the present study is two-fold. First, we extend the previous work by a comprehensive investigation of the effects of membrane thickness, drug binding and pH on the backbone conformation of a large number of residues in M2TM. The conformational changes were detected through ^{13}C and ^{15}N isotropic chemical shifts obtained from 2D MAS-NMR correlation spectra. We measured the chemical shifts of the contiguous stretch of residues from L26 to L38, and identified significant chemical shift changes at V27, S31, G34 and H37, which are pore-lining residues essential for drug inhibition and proton conduction [27,28]. While the chemical shift behavior of V27, S31 and G34 under a subset of these conditions has been reported before [21,22], they have not been systematically examined and compared. The H37 ^{13}C chemical shifts are entirely new and give information on the pH activation of the channel. These chemical shifts yield several new insights into the nature of the conformational changes of M2TM: 1) the conformational changes are coupled

among many residues; 2) different environmental factors may exert the same or opposite effects on the protein structure; and 3) the environmental parameters shift the protein conformational equilibrium among a small number of distinct states, so that more than one conformation usually exists under a certain condition. Based on the NMR chemical shifts, we obtained the backbone torsion angles of M2TM in three basis states, which correspond to the drug-bound protein at high pH in thick lipid bilayers, the drug-free protein at high pH in thin lipid bilayers, and the low-pH apo protein in thick lipid bilayers.

Materials and Methods

Membrane sample preparation

M2TM corresponding to the Udorn strain of influenza A virus (residues 22 46, SSDPLVVAASII GILHLILWILDRL) was synthesized using Fmoc chemistry by PrimmBiotech (Cambridge, MA) and purified to >95% purity. Several samples containing uniformly ^{13}C, ^{15}N-labeled residues from Leu26 to Leu38, Ile42 and Asp44 were used.

The lipid membranes used to reconstitute M2TM include DLPC (12:0) bilayers, DMPC (14:0) bilayers, and a mixed membrane that mimics the virus-envelope lipid composition [22]. The mixed membrane includes egg sphingomyelin (SM), DPPC, DPPE and cholesterol (Chol) at a molar ratio of 28% : 21% : 21% : 30%. For the viral membrane mixture, SM was first dissolved in chloroform/methanol (10 : 2) solution, then mixed with the other lipids and cholesterol in chloroform to the desired molar ratio. All membranes were lyophilized and then dissolved in a buffer of suitable pH, vortexed, and freeze-thawed several times to form large unilamellar vesicles. We used a pH 4.5 citrate buffer, a pH 7.5 phosphate buffer, and a pH 8.5 Tris buffer, for the various samples.

M2TM was reconstituted into the lipid membranes by detergent dialysis as described before [22,29]. The peptide : lipid molar ratios were 1: 15 1 : 12. The proteoliposomes were centrifuged at 150,000 g to obtain membrane pellets, which were then packed into 4 mm MAS rotors for NMR experiments. Photometric assay showed >95% binding of the peptide. For drug-bound samples, amantadine hydrochloride or 3-azaspiro[5,5]undecane hydrochloride was dissolved in buffer and directly titrated into the membrane.

Solid-state NMR experiments

Solid-state NMR experiments were carried out on a 400 MHz (9.4 Tesla) and a 600 MHz (14.1 Tesla) Bruker spectrometer using 4 mm MAS probes. Spectra of most viral membrane samples were measured near 303 K, while spectra of DLPC and DMPC-bound protein samples were measured at 243 K to freeze M2TM motion [23,30]. 2D ^{13}C-^{13}C DARR [31] correlation spectra were measured under 5 and 7 kHz MAS with a spin diffusion mixing time of 20 or 40 ms. 2D ^{15}N-^{13}C correlation spectra were measured under 7 kHz MAS using a REDOR sequence with 0.7 ms of ^{13}C-^{15}N coherence transfer [32]. Typical radio-frequency fields were 50 kHz for ^{13}C and ^{15}N and 60-70 kHz for ^{1}H. ^{13}C and ^{15}N chemical shifts were referenced to the α-Gly CO signal at 176.49 ppm on the TMS scale and the ^{15}N signal of N-acetyl-valine at 122 ppm on the liquid ammonia scale, respectively. After adjusting the ^{13}C chemical shifts to be referenced with respect to DSS (1.7 ppm larger values than the TMS-referenced chemical shifts [33]), we inputted the measured ^{13}C and ^{15}N isotropic shifts into TALOS+ [34] to obtain the backbone (ϕ, ψ) torsion angles. These torsion angles were used to generate the helix conformational models in Figure 6.

Results

Effects of membrane thickness, amantadine, and pH on chemical shifts

To examine how membrane thickness, drug, and pH affect the conformation of individual residues, we measured the ^{13}C and ^{15}N chemical shifts using 2D ^{13}C-^{13}C and ^{15}N-^{13}C correlation experiments. We first compared the M2TM spectra in three lipid bilayers: DLPC with 12 carbons per acyl chain, DMPC with 14 carbons per chain, and a cholesterol- and SM-containing virus-mimetic membrane with 16 or 18 carbons per chain. Figure 1A-C shows regions of the 2D ^{13}C-^{13}C and ^{15}N-^{13}C spectra of M2TM at pH 7.5 without amantadine. The DLPC and DMPC samples were measured at low temperature (243 K) to freeze the backbone motion [23, 30] while the viral-membrane samples were measured at 303 K since the backbone is already immobilized at ambient temperature [22]. L26, A29 and A30 exhibited a single set of chemical shifts independent of the membrane thickness. In contrast, two sets of chemical shifts with varying intensity ratios were observed for G34. We denote the set of peaks with larger ^{13}CO and ^{15}N chemical shifts as state 1, and the set of peaks with smaller ^{13}CO and ^{15}N chemical shifts as state 2. Peak area integration showed that the relative amounts of states 1 and 2 differed in the three membranes. In the thinnest membrane, DLPC, the percentage of state 1 was about ~25% of the total intensity. As the membrane thickness increased, the state-1 peak intensities increased. In DMPC membranes, state 1 accounted for ~56% of the total intensities, while in the thickest viral membrane, state 1 represented ~67% of the total population. V27 also showed bimodal conformational distribution, although the relative amounts of the two conformations varied less significantly with membrane thickness.

Upon binding of amantadine and 3-azaspiro [5,5] undecane hydrochloride [35], the 2D spectra showed higher state-1 intensities and lower state-2 intensities compared to the apo state in all three membranes. In the viral membrane, G34 now exhibited only the state-1 signals (Figure 1F), while in DMPC bilayers the dominant V27 signals also belonged to state 1 (Figure 1E). The other four sites, L26, A29, A30 and I35 displayed the same chemical shifts as the apo samples, indicating that their backbone conformation was insensitive to drug binding.

The shift of conformational equilibrium from state 2 to state 1 by drug binding gave a decisive clue to the nature of the two distinct backbone conformations. ^{15}N anisotropic chemical shifts of M2TM oriented in DMPC/DMPG bilayers indicated that amantadine binding caused a distinct helical kink at G34: the C-terminal segment became tilted by 20° from the bilayer normal whereas the N-terminal segment was tilted by 31° [36]. This kink was also reproduced in MD simulations of M2TM [37]. We thus assigned state 1, which was promoted by both drug binding and thick bilayers, to the discrete G34-kinked conformation. The state-2 conformation was promoted by thin bilayers and the absence of drugs. The tilt angle of the M2TM helices in DLPC bilayers in the absence of the drug was previously measured to be 35° using ^{15}N NMR of unoriented membranes [21]. However, these experiments probed only a small number of labeled residues that lie in the N-terminal segment of G34, thus, no information about the C-terminal orientation was known. Oriented-membrane ^{15}N NMR measurements on a larger number of labeled residues found that M2TM adopted a similar tilt angle of 35° in DMPC bilayer in the absence of drug [38]. However, the pH of these oriented samples was uncontrolled, and the membrane samples were deposited onto the glass plates from organic solution [38], making it possible that the peptide orientation was measured under acidic pH. Thus, the orientation of apo M2TM at high pH in thin lipid bilayers, and whether any kink exists at G34 in this state, is not yet known experimentally. We thus only assign state 2 to a conformation with likely larger tilt angles than for state 1, but do not specify the G34 conformation.

The effects of pH on the M2TM conformation are shown in Figure 2. The ^{13}C and ^{15}N chemical shifts were measured at pH 7.5 and pH 4.5 in the viral membrane. L26, V28, A29 and I32 exhibited the same chemical shifts at both pH, indicating that their conformation was unaffected by pH. As in Figure 1C, V27 and G34 exhibited dual conformations at pH 7.5. Upon lowering the pH to 4.5, V27 and G34 displayed only a single set of chemical shifts, which was designated as state 3. The state-3 V27 had a 1.6 ppm larger Cα chemical shift and a counter-directional 1.6 ppm smaller CO chemical shift (Table 1) compared to the high-pH state 1. These low-pH values are similar to the state-2 chemical shifts of V27, which were obtained in thin bilayers at high pH. For G34, the low-pH state 3 chemical shifts are moderately larger for Cα (0.8 ppm) while the CO and ^{15}N chemical shifts are significantly smaller (2.1 ppm and 2.6 ppm, respectively) than the state-1 chemical shifts (Table 1), but are similar to the state-2 chemical shifts (Figure 1). In addition to these individual chemical shift changes, V27 and G34 peaks broadened significantly at low pH compared to the high-pH state 1: the ^{13}C and ^{15}N linewidths increased by an average of 0.9 ppm and 0.6 ppm, respectively, compared to the apo peptide in the viral membrane. This line broadening indicates that the low-pH state-3 conformational distribution is a single Gaussian with a large width [39], in contrast to the narrowly peaked conformational distribution of state 1 at high pH.

S31 is the closest residue to amantadine in the drug-complexed peptide [16,29] and was shown to increase its ^{15}N chemical shift by a striking 7 ppm from the apo state in DLPC bilayers [30]. Interestingly, S31 chemical shifts also exhibited pH sensitivity, as seen in the spectra for viral-membrane samples (Figure 2C, D): low pH increased the S31 Cα and CO chemical shifts while decreasing the ^{15}N chemical shift by ~ 4 ppm compared to the apo peptide in the viral membrane at high pH. Based on the secondary-structure dependent chemical shift trends [40], these changes suggest that the S31 backbone became more ideally helical at low pH.

Histidine 37 is the proton-gating residue of the M2 channel [14] and is thus expected to have large conformational dependence on pH. Figure 3 compares the spectra of G34, H37 and I42 labeled M2TM at pH 8.5 and pH 4.5 in the viral membrane. Similar to V27 and G34, H37 exhibited two well-defined conformations at high pH and only a single, but broadly distributed, conformation at low pH. The two high-pH conformations differ by 2.7 ppm in the Cβ chemical shift. We did not measure the spectra of amantadine-bound H37. However, since all other porelining residues show the dominant conformation in the viral membrane to be identical to the amantadine-induced conformation, we tentatively attribute the main Cβ chemical shift of 30.6 ppm (Table 1) to the state caused by amantadine, which is state 1. The minor peak at 27.9 ppm is attributed to state 2, which is expected to be present at higher amounts in thin membranes in the absence of the drug.

Compared to the dominant chemical shifts at pH 8.5, lowering the pH changed the H37 pH 4.5 Cα and Cβ chemical shifts counter-directionally: the Cα chemical shift increased by 2.1 ppm while the Cβ chemical shift decreased by a large 4.4 ppm (Table 1). These changes indicate a more ideal α-helical conformation for H37 at low pH. Smaller changes of CO and ^{15}N chemical shifts were also observed. In addition to the H37 chemical shift changes, the pH 8.5 spectra also showed a higher fraction of G34 in state 1 compared to its fraction at pH 7.5 (Figure 1), suggesting that the effect of pH on the protein conformation equilibrium is incremental: the higher the pH, the larger amount of state-1 conformation.

The chemical shift changes of V27, G34 and H37 shown in Figures 1-3 are coupled, in the sense that the signals of multiple residues in the same state change collectively with the environment. Moreover, the chemical shifts under a certain combination of conditions are the superposition of the three basis conformations identified here. The effects of multiple

external parameters on the protein conformation are additive. For example, when thick bilayers, high pH and drug binding are combined, M2TM is almost exclusively in state 1 (Figure 1C). The corollary of this statement is that counter-acting external parameters cause a mixture of conformations. For example, the drug-complexed M2TM in thin bilayers at high pH (Figure 1D) shows a roughly equimolar mixture of state-1 and state-2 conformations.

Table 1 lists the chemical shifts of the three basis states for the four environment-sensitive pore-lining residues: V27, S31, G34 and H37. Because Table 1 lists only basis-state chemical shifts, not all chemical shifts observed in the spectra are included. For example, the apo-peptide chemical shifts in the viral membrane at high pH (Figure 2C) are intermediate between the state 1 and state 2 values, and are not represented in Table 1. Inspection of the chemical shifts confirms that state 2 and state 3 are similar for the first three residues, while H37 shows distinct chemical shifts between the high-pH state 2 and the low-pH state 3.

Figure 4 depicts the effects of membrane thickness, drug binding, and pH on the M2TM conformation. In DLPC bilayers at high pH, the apo M2TM mainly adopts the state-2 conformation, which is characterized by non-ideal helical conformation at H37 and likely a large average tilt angle (Figure 4A). Several lines of evidence suggest that the G34 conformation in state 2 is heterogeneous, containing both highly kinked and relatively straight conformations. First, the state-2 G34 peaks are always broader than in state 1 (Figure 1). Second, MD simulations of the apo peptide found the presence of both large and no kink angles at G34 [37]. Third, TALOS torsion angles derived from the measured isotropic chemical shifts (see below) resulted in a state-2 α-helix with an average kink of 10° at G34, which is larger than the kink found in state 1. As the bilayer thickness increases, the state-1 conformation becomes dominant (Figure 4B,C). This state has a well-defined G34 kink and similarly non-ideal H37 torsion angles, and the helix may be less tilted than in DLPC bilayers to better match the hydrophobic thickness of the membrane. In Figure 4, we represent the well-defined G34 kink in the drug-bound state 1 as a break in the helical rod, while denoting the distribution of G34 conformation in state 2 as two C-terminal helical rods with different orientations with respect the N-terminal segment. We depict and the non-ideal conformation of H37 at high pH as small wiggles in the helical rod. Drug binding, similar to thick bilayers, shifts the conformational equilibrium to state 1, and when the drug binds to the protein in the thick virus-mimetic membrane, state-1 conformation is the only one observed. In comparison, the drug-free M2TM in the thick membrane adopts both state-1 and state-2 conformations (Figure 4D). Upon lowering of pH, M2TM adopts more ideal helical conformation at H37 (Figure 4E). Although state 3 shows only a single averaged structure, the larger spectral linewidths suggest that small conformational fluctuations abound, which is represented here by a blurred helical rod. These conformational fluctuations may support proton conduction by providing the conformational flexibility necessary to conduct protons.

M2TM torsion angles and helix conformations in three basis states

To obtain more quantitative information about the helical structure of M2TM in various states, we inputted the conformation-dependent Cα, Cβ, CO and ^{15}N chemical shifts into the TALOS+ program [34] to calculate the average (ϕ, ψ) torsion angles. Figure 5 and Table 2 give the torsion angles for residues 26 43 in the three conformational states. No chemical shifts were available for the segment from I39 to W41, thus we used the (ϕ, ψ) angles obtained from orientation and distance constraints [16,36] for all three basis states. We found that state 2, which is promoted by thin lipid bilayers and no drug, shows similar torsion angles as the low-pH state 3. State 1, promoted by thick membranes and drug binding, differ significantly from the other two states at S31, G34 and I35. The L36-H37 segment shows the largest (ϕ, ψ) angle differences among the three states: the low-pH state 3

exhibits the most ideal (ϕ, ψ) angles of (−64°, −43°), while the drug-bound high-pH state 1 has (ϕ, ψ) angles of (−79°, −31°). This result is interesting, as it indicates that amantadine binding at S31 perturbs the conformation of the pH-activation residue two helical turns away. This drug-induced conformational change is qualitatively consistent with the measured perturbation of the H37 pKa by amantadine [41]. At low pH, electrostatic repulsion pushes the four helices apart, relieving steric hindrance and allowing the H37 tetrad to adopt more ideal torsion angles. At high pH, drug binding favors a kink at G34, which reduces the distance among the four neutral imidazoles, allowing them to interact strongly with each other [42].

Figure 6 shows the helical conformations of the three basis states obtained from the chemical-shift constrained (ϕ, ψ) angles. The three monomers are oriented to reflect the approximate tilt angle in lipid bilayers, and the channel axis is approximately the vertical axis away from the H37 imidazole rings. Using the average N-H vector orientations for residues 27-33 and residues 36-42, we found that the kink angle at G34 was 6.6° for state 1, 10.1° for state 2, and 9.4° for state 3. Thus, the low-pH state 3 and the high-pH thin-membrane state 2 actually contain slightly larger kinks at G34. However, the kink occurs in different directions from the drug-complexed state-1 conformation (Figure 6). Aligning the N-terminal segments for all three states, we found that the C-terminal helix orientations are 11° apart between states 1 and 2, and similarly 11° apart between states 1 and 3, but only 2° different between state 2 and state 3. Superposition of the helices shows the deviation of the C-terminal orientation between state 1 and the other two states.

Discussion

Helix kink at G34

The conformational plasticity of M2TM has been noted before in various experiments. Uniaxially aligned M2TM on glass plates showed that the membrane reconstitution protocol, amantadine, and pH can all affect the peak positions and linewidths of the ^{15}N anisotropic spectra [20]. Amantadine binding caused a well-defined kink at G34 [36], whereas decreasing the pH mainly increased the protein conformational distribution. The low-pH induced increase of the conformational distribution was also reported for DHPC micelle-bound M2(18-60) studied by solution NMR [19].

The MAS spectra obtained here provide further insights into the nature of the M2TM conformational plasticity. The isotropic chemical shifts directly indicate the backbone (ϕ, ψ) angles, thus they probe the degree of helix ideality under various environmental conditions. The spectra in Figure 1 showed that the V27, S31, and G34 underwent coupled conformational changes with drug binding and membrane thickness. Increasing the membrane thickness produced similar effects as drug binding. The state 1 that is favored by drug binding is characterized by less ideal helical torsion angles for G34. This G34 non-ideality is consistent with the oriented ^{15}N NMR result [36], but our data further reveals that the kinked G34 conformation is already present in the apo state, since state-1 signals are already manifested in the apo membrane spectra in Figure 1A-C.

The helical kink at G34 was recently examined in more detail by MD simulations that reproduced the oriented solid-state NMR ^{15}N spectra [37]. It was found that in DMPC bilayers at high pH, apo M2TM exhibited two populations of conformations: ~35% of the peptide showed large kink angles of 25-50° at G34, while ~65% major fraction exhibited a straight helix with no kink. In comparison, the amantadine-bound peptide exhibited a uniform kink angle of ~10° at G34. Thus, these simulations predicted three G34 conformations, an ideal helix with no kink (0°), a narrowly distributed and small kink of 10°, and a broadly distributed kink at much larger angles. Our apo-peptide spectra show two

distinct sets of G34 peaks, where the set with narrower linewidths is identical to the drug-bound peaks. We attribute the set of broader peaks (state 2) to the combination of straight and significantly kinked conformations seen in the MD simulations, since the larger linewidths are consistent with the broad distribution of kink angles.

It is generally known that membrane peptides adapt their orientations in lipid membranes to minimize the hydrophobic mismatch with the lipid bilayer [43,44], so that a thicker bilayer might be expected to promote straight helices with small tilt angles. Thus, the presence of a distinct kink in M2TM bound to the thick viral membrane may appear at first surprising. However, the kink needs not contradict a smaller tilt angle or a larger hydrophobic length along the bilayer normal. In the amantadine-bound M2TM structure, the C-terminal segment is much less tilted (20°) than the average tilt angle of 35° for the apo peptide [36]. If we assume that the same conformation is applicable to the thick membrane, as suggested by the similar chemical shifts between the two states, then the direction of the G34 kink actually increases the hydrophobic length of the peptide in the thick membrane, thus reducing the hydrophobic mismatch with the bilayer. Therefore, whether helical kinks are favorable for reducing hydrophobic mismatch depend on whether the kinks cause part of the helices to adopt larger or smaller tilt angles. For the same reason, the TALOS-predicted kink angle of 10° for state 2, found in thin lipid bilayers, is not surprising, because the kink has an opposite direction to that of state 1 such that it should cause a larger tilt angle for the C-terminal segment and thus decrease the hydrophobic thickness of the peptide.

Interestingly, a kink in the transmembrane helix of the HIV virus Vpu protein, observed in oriented ^{15}N NMR spectra [45] was present in DOPC bilayers (18:1 chains) but absent in thinner bilayers. Moreover, the kinked residue, I17, also lies in the middle of the helix, similar to the position of G34 in M2TM. At present we do not fully understand the origin of kink formation in the middle of transmembrane helices. Elucidation of this phenomenon will likely require consideration of multiple factors, such as the type and position of the anchoring residues [46], lateral pressure and viscosity distributions within the bilayer [30], and the amino acid sequence of the protein. The last aspect is relevant because the structure of oligomeric ion channels is not only influenced by protein-lipid interactions but also by protein-protein interactions that are required to maintain function.

V27 and S31 conformations

State 1 exhibits less ideal helical chemical shifts for V27 (Table 2), which is most likely due to the interaction of V27 sidechains with amantadine, as shown by recent distance measurements between amantadine and V27 [16]. This less ideal V27 conformation is consistent with an MD simulation that suggested V27 to act as a secondary gate for amantadine, forming an extended blockage of the water wire in the channel pore in the presence of the drug [47].

Decreasing the membrane thickness and removing amantadine shifted the conformational equilibrium to state 2, which has more ideal helical conformations for V27. Interestingly, state 2 was not found by itself under any of the experimental conditions used here, but always coexisted with state 1, while the discretely kinked state-1 conformation can be isolated by using thick lipid bilayers and adding amantadine. Thiol-disulfide exchange experiments showed that the M2TM tetramers are significantly stabilized in thicker bilayers containing cholesterol [48], indicating that the discretely kinked state 1 corresponds to the thermodynamically more stable conformation. Since cholesterol and palmitoyl-chain lipids are also the main ingredients of virus envelope membranes [22], while 12-carbon lipid chains are uncommon, the state-1 conformation is also likely the more functional structure than state 2 at high pH.

The S31 Cβ chemical shift in various states is noteworthy: it is similar to Cα chemical shift in states 2 and 3, but 1.5 ppm upfield from Cα in the drug-bound state 1 (Table 1). Although the similar S31 Cα and Cβ chemical shifts make the signals more difficult to resolve than other residues in 2D spectra, spectral editing experiments that suppressed the CH signals while selectively detecting the CH_2 signals confirmed these Cβ chemical shift values [29,49]. The slightly upfield Cβ chemical shift in state 1 deviates from the database average, which shows the Cβ chemical shift to be larger than Cα in both α-helical and β-sheet conformations [50,51]. Since the Cβ chemical shift is significantly influenced by the hydroxyl oxygen in addition to (ϕ, ψ) angles, we attribute the upfield Cβ shift in state 1 to perturbations of the hydroxyl environment by drug binding. ^{1}H spin diffusion experiments from water to the protein [52] clearly indicate that amantadine, which binds at S31 [16], significantly dehydrates the channel, which should remove H-bonding between the hydroxyl and water molecules. The increased electron density at the OH should increase the shielding of Cβ, thus causing a smaller chemical shift. Among the three states, the Cβ chemical shift is closest to the ideal α-helical value in the state 3. This is consistent with the better hydration of the channel at low pH, which should allow extensive hydroxyl-water H-bonding [18,52,53], thus causing a deshielding effect on Cβ. Thus, the Cβ chemical shift variation among the three states, while subtle, is consistent with the expected structural changes of the channel at this important residue.

H37 conformation and the influence of pH

H37 backbone conformation showed significant non-ideality at high pH (Figure 3). The predicted (ϕ, ψ) angles were (−79°, −31°) for state 1 and (−69°, −38°) for state 2. The average (ϕ, ψ) angles of α-helices in water-soluble proteins are (−65°, −40°) [54], while the ideal torsion angles of transmembrane α-helices were predicted to be (−60°, −45°) [55,56]. The 5° counter-directional change in the (ϕ, ψ) torsion angles has been proposed to have a significant effect on the electrostatic surface of α-helices [57], by better shielding the polar carbonyl groups from the hydrophobic environment of the membrane. The high-pH torsion angles of H37 are 15-20° different from the ideal torsion angles for transmembrane α-helices, and are closer to the values for water-soluble helices. The neighboring residues L36 and L38, influenced by H37, also exhibited non-ideal (ϕ, ψ) angles, although not as strongly as H37. For all three residues, the strongly negative f angles and the less negative y angles translate to larger angles between adjacent peptide planes [57] and suggest that the carbonyl oxygens are less well hydrogen-bonded to their intra-helical partners but more exposed to the solvent. Based on this observation, we hypothesize that the deviation of the high-pH H37 conformation from an ideal transmembrane a-helix may result from either intermolecular H-bonding of the H37 carbonyl with water molecules, or aromatic interactions among the four histidines due to tight inter-helical packing at high pH [58].

Lowering the pH moved the H37 Cα chemical shift downfield and the Cβ chemical shift upfield (Table 1), indicating a more ideal helical conformation (Figure 5). This more ideal backbone is consistent with opening of the channel at this position due to the electrostatic repulsion of the positively charged imidazolium at low pH [58]. Indeed, X-ray crystal structures of M2TM as a function of pH [18,53] showed that the C-terminal helices increasingly move apart from each other at lower pH, facilitating proton conduction into the cell.

At low pH, MD simulations found that the large-kink population at G34 became more populated, which was interpreted as facilitating proton conduction by creating a wider pore at the H37-W41 juncture. Our chemical shift data show that the low-pH G34 chemical shifts (state 3) are nearly the same as the apo G34 chemical shifts at high pH (state 2), thus supporting this prediction.

Conformational difference between lipid-facing and pore-lining residues

The chemical-shift-constrained (ϕ, ψ) torsion angles in Figure 5 and Table 2 reveal the interesting trend that lipid-facing residues V28, A29, I32 and I33 adopt (ϕ, ψ) angles expected for transmembrane α-helices, with less negative ϕ angles and more negative ψ angles. The average state-1 (ϕ, ψ) angles for the lipid-facing residues are (−62°, −42°), whereas the pore-facing residues V27, A30, S31, G34 and H37 have average (ϕ, ψ) angles of (−70°, −38°) in state 1, closer to the values for water-soluble helices. This difference suggests the sensitivity of isotropic chemical shifts to ~5° changes in the torsion angles, due to changes in the local dielectric environment faced by the residues in this TM helical bundle.

This study shows the sensitivity of NMR chemical shifts to membrane protein conformations. With the availability of increasingly sopHisticated structure prediction methodologies [59], it will be worthwhile to investigate the folding and conformational transitions of oligomeric membrane proteins at higher resolution using chemical shifts as the main input [60]. The general difficulties of measuring intermolecular and intramolecular distances in homo-oligomeric membrane proteins provide further incentives to using chemical shifts as the main experimental input for mapping out conformational changes under a wide range of conditions.

Acknowledgments

This work was funded by an NSF grant MCB-0543473 and an NIH grant GM088204.

References

1. Long SB, Tao X, Campbell EB, MacKinnon R. Atomic Structure of a Voltage-Dependent K+ Channel in a Lipid Membrane-Like Environment. Nature 2007;450:376–383. [PubMed: 18004376]
2. Brejc K, van Dijk WJ, Klaassen RV, Schuurmans M, van Der Oost J, Smit AB, Sixma TK. Crystal structure of an ACh-binding protein reveals the ligand-binding domain of nicotinic receptors. Nature 2001;411:269–276. [PubMed: 11357122]
3. Engelman DM. Crossing the hydrophobic barrier: insertion of membrane proteins. Science 1996;274:1850–1851. [PubMed: 8984645]
4. Slatin SL, Qiu X, Jakes KS, Finkelstein A. Identification of a translocated protein segment in a voltage-dependent channel. Nature 1994;371:158–161. [PubMed: 7521016]
5. Parker MW, Pattus F, Tucker AD, Tsernoglou D. Structure of the membrane-poreforming fragment of colicin A. Nature 1989;337:93–96. [PubMed: 2909895]
6. Vásquez V, Sotomayor M, Cordero-Morales J, Schulten K, Perozo E. A structural mechanism for MscS gating in lipid bilayers. Science 2008;321:1210–1214. [PubMed: 18755978]
7. Bass RB, Strop P, Barclay M, Rees DC. Crystal structure of Escherichia coli MscS, a voltage-modulated and mechanosensitive channel. Science 2002;298:1582–1587. [PubMed: 12446901]
8. Spencer RH, Rees DC. The alpha-helix and the organization and gating of channels. Annu. Rev. Biophys. Biomol. Struct 2002;31:207–233. [PubMed: 11988468]
9. Mitra A, Tascione R, Auerbach A, Licht S. Plasticity of acetylcholine receptor gating motions via rate-energy relationships. Biophys J 2005;89:3071–3078. [PubMed: 16113115]
10. Dill KA, Chan HS. From Levinthal to pathways to funnels. Nat. Struct. Biol 1997;4:10–19. [PubMed: 8989315]
11. Pinto LH, Lamb RA. Controlling influenza virus replication by inhibiting its proton flow. Mol. BioSyst 2007;3:18–23. [PubMed: 17216051]
12. Pinto LH, Holsinger LJ, Lamb RA. Influenza virus M2 protein has ion channel activity. Cell 1992;69:517–528. [PubMed: 1374685]
13. Wang C, Takeuchi K, Pinto LH, Lamb RA. Ion Channel Activity of Influenza A Virus M2 Protein: Characterization of the Amantadine Block. J. Virol 1993;67:5585–5594. [PubMed: 7688826]

14. Wang C, Lamb RA, Pinto LH. Activation of the M2 ion channel of influenza virus: a role for the transmembrane domain histidine residue. Biophys. J 1995;69:1363–1371. [PubMed: 8534806]
15. Tang Y, Zaitseva F, Lamb RA, Pinto LH. The Gate of the Influenza Virus M2 Proton Channel Is Formed by a Single Tryptophan Residue. J. Biol. Chem 2002;277:39880–39886. [PubMed: 12183461]
16. Cady SD, Schmidt-Rohr K, Wang J, Soto CS, DeGrado WF, Hong M. Structure of the amantadine binding site of influenza M2 proton channels in lipid bilayers. Nature 2010;463:689–692. [PubMed: 20130653]
17. Ma C, Polishchuk AL, Ohigashi Y, Stouffer AL, Schon A, Magavern E, Jing X, Lear JD, Freire E, Lamb RA, DeGrado WF, Pinto LH. Identification of the Functional Core of the Influenza A Virus A/M2 Proton-Selective Ion Channel Proc. Natl. Acad. Sci. U.S.A 2009;106:12283–12288.
18. Stouffer AL, Acharya R, Salom D, Levine AS, Di Costanzo L, Soto CS, Tereshko V, Nanda V, Stayrook S, DeGrado WF. Structural basis for the function and inhibition of an influenza virus proton channel. Nature 2008;451:596–599. [PubMed: 18235504]
19. Schnell JR, Chou JJ. Structure and mechanism of the M2 proton channel of influenza A virus. Nature 2008;451:591–595. [PubMed: 18235503]
20. Li C, Qin H, Gao FP, Cross TA. Solid-state NMR characterization of conformational plasticity within the transmembrane domain of the influenza A M2 proton channel. Biochim. Biophys. Acta 2007;1768:3162–3170. [PubMed: 17936720]
21. Cady SD, Hong M. Amantadine-induced conformational and dynamical changes of the influenza M2 transmembrane proton channel. Proc. Natl. Acad. Sci. U.S.A 2008;105:1483–1488. [PubMed: 18230730]
22. Luo W, Cady SD, Hong M. Immobilization of the Influenza A M2 Transmembrane Peptide in Virus-Envelope Mimetic Lipid Membranes: A Solid-State NMR Investigation. Biochemistry 2009;48:6361–6368. [PubMed: 19489611]
23. Cady SD, Goodman C, Tatko C, DeGrado WF, Hong M. Determining the orientation of uniaxially rotating membrane proteins using unoriented samples: a 2H, 13C, and 15N solid-state NMR investigation of the dynamics and orientation of a transmembrane helical bundle. J. Am. Chem. Soc 2007;129:5719–5729. [PubMed: 17417850]
24. Duong-Ly KC, Nanda V, DeGrado WF, Howard KP. The conformation of the pore region of the M2 proton channel depends on lipid bilayer environment. Protein Sci 2005;14:856–861. [PubMed: 15741338]
25. Stouffer AL, Ma C, Cristian L, Ohigashi Y, Lamb RA, Lear JD, Pinto LH, DeGrado WF. The interplay of functional tuning, drug resistance, and thermodynamic stability in the evolution of the M2 proton channel from the influenza A virus. Structure 2008:1067–1076. [PubMed: 18611380]
26. Howard KP, Lear JD, DeGrado WF. Sequence determinants of the energetics of folding of a transmembrane four-helix-bundle protein. Proc. Natl. Acad. Sci. USA 2002;99:8568–8572. [PubMed: 12084917]
27. Balannik V, Carnevale V, Fiorin G, Levine BG, Lamb RA, Klein ML, Degrado WF, Pinto LH. Functional studies and modeling of pore-lining residue mutants of the influenza a virus M2 ion channel. Biochemistry 2010;49:696–708. [PubMed: 20028125]
28. Cady SD, Luo WB, Hu F, Hong M. Structure and function of the influenza M2 proton channel. Biochemistry 2009;48:7356–7364. [PubMed: 19601584]
29. Cady SD, Mishanina TV, Hong M. Structure of amantadine-bound M2 transmembrane peptide of influenza A in lipid bilayers from magic-angle-spinning solid-state NMR: the role of Ser31 in amantadine binding. J. Mol. Biol 2009;385:1127–1141. [PubMed: 19061899]
30. Cady SD, Hong M. Effects of Amantadine Binding on the Dynamics of Bilayer-Bound Influenza A M2 Transmembrane Peptide Studied by NMR Relaxation. J. Biomol. NMR 2009;45:185–196. [PubMed: 19633911]
31. Takegoshi K, Nakamura S, Terao T. C-13-H-1 dipolar-assisted rotational resonance in magic-angle spinning NMR. Chem. Phys. Lett 2001;344:631–637.
32. Hong M, Griffin RG. Resonance assignments for solid peptides by dipolar-mediated C-13/N-15 correlation solid-state NMR. J. Am. Chem. Soc 1998;120:7113–7114.

33. Wishart DS, Bigam CG, Holm A, Hodges RS, Sykes BD. 1H, 13C and 15N random coil NMR chemical shifts of the common amino acids. I. Investigations of nearest neighbor effects. J. Biomol. NMR 1995;5:67–81. [PubMed: 7881273]
34. Shen Y, Delaglio F, Cornilescu G, Bax A. TALOS+: a hybrid method for predicting protein backbone torsion angles from NMR chemical shifts. J. Biomol. NMR 2009;44:213–223. [PubMed: 19548092]
35. Wang J, Cady SD, Balannik V, Pinto LH, DeGrado WF, Hong M. Discovery of spiro-piperidine inhibitors and their modulation of the dynamics of the M2 proton channel from influenza A virus. J. Am. Chem. Soc 2009;131:8066–8076. [PubMed: 19469531]
36. Hu J, Asbury T, Achuthan S, Li C, Bertram R, Quine JR, Fu R, Cross TA. Backbone structure of the amantadine-blocked trans-membrane domain M2 proton channel from Influenza A virus. Biophys. J 2007;92:4335–4343. [PubMed: 17384070]
37. Yi M, Cross TA, Zhou HX. Conformational heterogeneity of the M2 proton channel and a structural model for channel activation. Proc. Natl. Acad. Sci. U. S. A 2009;106:13311–13316. [PubMed: 19633188]
38. Wang J, Kim S, Kovacs F, Cross TA. Structure of the transmembrane region of the M2 protein H+ channel. Protein Sci 2001;10:2241–2250. [PubMed: 11604531]
39. Yao XL, Hong M. Structural Distribution in an Elastin-Mimetic Peptide (VPGVG)3 Investigated by Solid State NMR. J. Am. Chem. Soc 2004;126:4199–4210. [PubMed: 15053609]
40. Wishart DS, Sykes BD, Richards FM. Relationship between nuclear magnetic resonance chemical shift and protein secondary structure. J. Mol. Biol 1991;222:311–333. [PubMed: 1960729]
41. Hu J, Fu R, Cross TA. The chemical and dynamical influence of the anti-viral drug amantadine on the M2 proton channel transmembrane domain. Biophys. J 2007;93:276–283. [PubMed: 17434944]
42. Hu J, Fu R, Nishimura K, Zhang L, Zhou H-X, Busath DD, Vijayvergiya V, Cross TA. Histidines, heart of the hydrogen ion channel from influenza A virus: Toward an understanding of conductance and proton selectivity. Proc. Natl. Acad. Sci. USA 2006;103:6865–6870. [PubMed: 16632600]
43. Killian JA. Hydrophobic mismatch between proteins and lipids in membranes. Biochim. Biophys. Acta 1998;1376:401–415. [PubMed: 9805000]
44. de Planque MR, Boots JW, Rijkers DT, Liskamp RM, Greathouse DV, Killian JA. The effects of hydrophobic mismatch between phosphatidylcholine bilayers and transmembrane alpha-helical peptides depend on the nature of interfacially exposed aromatic and charged residues. Biochemistry 2002;41:8396–8404. [PubMed: 12081488]
45. Park SH, Opella SJ. Tilt angle of a trans-membrane helix is determined by hydrophobic mismatch. J. Mol. Biol 2005;350:310–318. [PubMed: 15936031]
46. de Planque MR, Bonev BB, Demmers JA, Greathouse DV, Koeppe R.E.n. Separovic F, Watts A, Killian JA. Interfacial anchor properties of tryptophan residues in transmembrane peptides can dominate over hydrophobic matching effects in peptide-lipid interactions. Biochemistry 2003;42:5341–5348. [PubMed: 12731875]
47. Yi M, Cross TA, Zhou HX. A secondary gate as a mechanism for inhibition of the M2 proton channel by amantadine. J. Phys. Chem. B 2008;112:7977–7979. [PubMed: 18476738]
48. Cristian L, Lear JD, DeGrado WF. Use of thiol-disulfide equilibria to measure the energetics of assembly of transmembrane helices in phospholipid bilayers. Proc. Natl. Acad. Sci. USA 2003;100:14772–14777. [PubMed: 14657351]
49. Mao JD, Schmidt-Rohr K. Methylene spectral editing in solid-state C-13 NMR by three-spin coherence selection. J. Magn. Reson 2005;176:1–6. [PubMed: 15941664]
50. Wang Y, Jardetzky O. Probability-based protein secondary structure identification using combined NMR chemical-shift data. Protein Sci 2002;11:852–861. [PubMed: 11910028]
51. Zhang H, Neal S, Wishart DS. RefDB: A database of uniformly referenced protein chemical shifts. J. Biomol. NMR 2003;25:173–195. [PubMed: 12652131]
52. Luo W, Hong M. Conformational changes of an ion channel membrane protein detected through water-protein interactions using solid-state NMR spectroscopy. J. Am. Chem. Soc 2010;132:2378–2384. [PubMed: 20112896]

53. Acharya A, Carnevale V, Fiorin G, Levine BG, Polishchuk A, Balannick V, Samish I, Lamb RA, Pinto LH, DeGrado WF, Klein ML. Structural mechanism of proton transport through the influenza A M2 protein. Proc. Natl. Acad. Sci. U. S. A 2010;107:15075–15080. [PubMed: 20689043]

54. Smith LJ, Bolin KA, Schwalbe H, MacArthur MW, Thornton JM, Dobson CM. Analysis of main chain torsion angles in proteins: prediction of NMR coupling constants for native and random coil conformations. J. Mol. Biol 1996;255:494–506. [PubMed: 8568893]

55. Blundell T, Barlow D, Borkakoti N, Thornton J. Solvent-induced distortions and the curvature of alpha-helices. Nature 1983;306:281–283. [PubMed: 6646210]

56. Kim S, Cross TA. Uniformity, ideality, and hydrogen bonds in transmembrane alpha-helices. Biophys. J 2002;83:2084–2095. [PubMed: 12324426]

57. Page RC, Kim S, Cross TA. Transmembrane helix uniformity examined by spectral mapping of torsion angles. Structure 2008;16:787–797. [PubMed: 18462683]

58. Hu F, Luo W, Hong M. Mechanisms of proton conduction and gating by influenza M2 proton channels from solid-state NMR. Science. 2010 in press.

59. Raman S, Lange OF, Rossi P, Tyka M, Wang X, Aramini J, Liu G, Ramelot TA, Eletsky A, Szyperski T, Kennedy MA, Prestegard J, Montelione GT, Baker D. NMR structure determination for larger proteins using backbone-only data. Science 2010;327:1014–1018. [PubMed: 20133520]

60. Havlin RH, Tycko R. Probing site-specific conformational distributions in protein folding with solid-state NMR. Proc. Natl. Acad. Sci. U. S. A 2005;102:3284–3289. [PubMed: 15718283]

61. Luo W, Mani R, Hong M. Sidechain conformation and gating of the M2 transmembrane peptide proton channel of influenza A virus from solid-state NMR. J. Phys. Chem 2007;111:10825–10832.

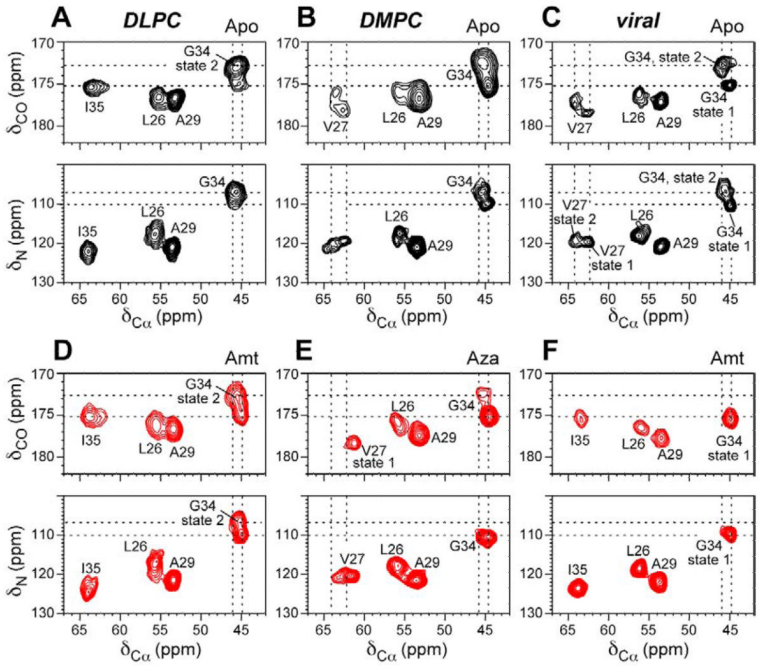

Figure 1.

M2TM chemical shift changes due to membrane thickness and drug binding from 2D ^{13}C-^{13}C and ^{15}N-^{13}C correlation spectra at pH 7.5. Apo spectra are shown in black and drug-bound spectra in red. **A**. Apo peptide in DLPC bilayers. **B**. Apo peptide in DMPC bilayers. **C**. Apo peptide in virus-mimetic membranes. **D**. Amantadine-bound peptide in DLPC bilayers. **E**. M2TM bound to 3-azaspiro[5,5]undecane hydrochloride (Aza) in DMPC bilayers. **F**. Amantadine-bound peptide in virus-mimetic membranes. The viral membrane spectra (C, F) were measured at 303 K, while the other spectra were measured at 243 K. The 2D ^{15}N-^{13}C spectra of DLPC and viral membrane samples were reproduced from [22].

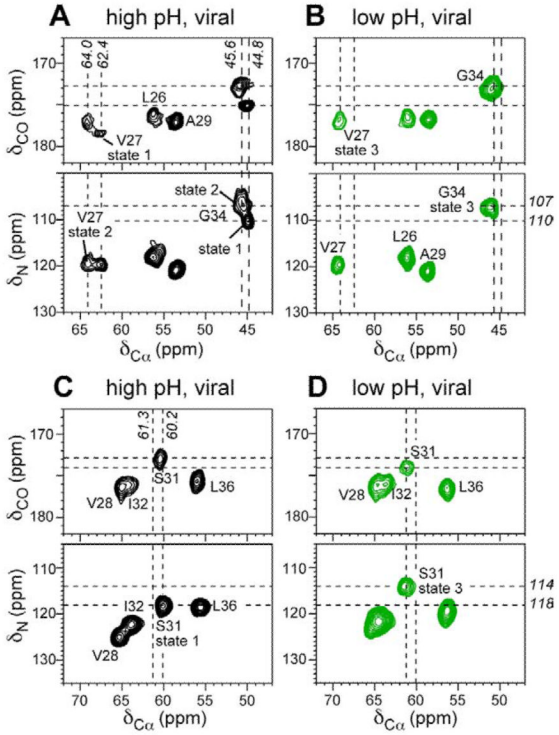

Figure 2.

2D ^{13}C-^{13}C and ^{15}N-^{13}C correlation spectra of viral-membrane-bound M2TM at pH 7.5 (black) and pH 4.5 (green). **A**. V27 and G34-containing M2TM spectra at pH 7.5 at 303 K (same as Figure 1C). **B**. V27 and G34-containing spectra at pH 4.5 at 303 K. **C**. S31-containing M2TM spectra at pH 7.5. **D**. S31-containing spectra at pH 4.5. Spectra (C, D) were measured at 273 K for the ^{13}C-^{13}C spectra and 243 K for the ^{15}N-^{13}C spectra.

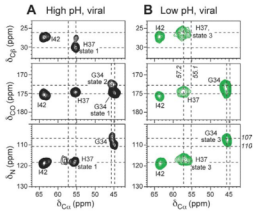

Figure 3.

His37 and G34 chemical shifts of viral-membrane-bound M2TM at pH 8.5 (**A**) and pH 4.5 (**B**), measured at 273 K. From top to bottom, the ^{13}Cα-^{13}Cβ region, the ^{13}CO-^{13}Cα region, and ^{15}N-^{13}Cα region of 2D spectra are plotted.

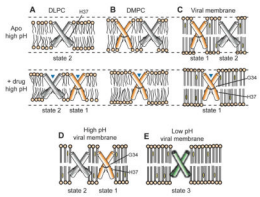

Figure 4.

Schematic of the effects of membrane thickness, drug binding and pH on M2TM conformation. For clarity only two of the four helices are drawn. **A**. DLPC bilayers. **B**. DMPC bilayers. **C**. Virus-mimetic bilayers. Top row: Without drug. Bottom row: With amantadine or 3-azaspiro[5,5]undecane hydrochloride. Dashed lines guide the eye for the bilayer thickness. Thicker membranes and drug binding promote a conformation with a well-defined G34 kink, which is shown as a break in the helical rod. Thin membranes and the absence of drug promote a broadly distributed conformation at G34, which is illustrated as two orientations of the helix C-terminal to G34. Non-ideal helical conformation at H37 is represented as small wiggles in the rods. **D**. High-pH conformation of M2TM in viral membranes. **E**. Low pH conformation of M2TM in viral membranes. Low pH promotes a more ideal helical conformation at H37 and increases the conformational distributions of the protein.

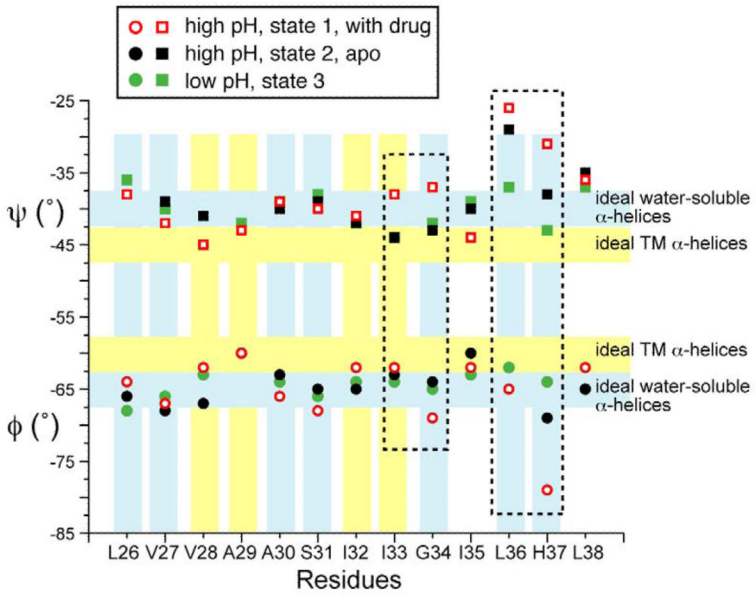

Figure 5.

(ϕ, ψ) torsion angles of three states of M2(22-46) constrained by isotropic ^{13}C and ^{15}N chemical shifts using TALOS+ [34]. The largest torsion angle changes are observed at G34 and H37. Yellow bars indicate torsion angles of ideal transmembrane helices (horizontal) and residues that fall into this category (vertical), which are predominantly lipid-facing residues in M2TM. Blue bars indicate the torsion angles of ideal water-soluble helices (horizontal) and residues that fall into this category (vertical), which are mostly pore-lining residues.

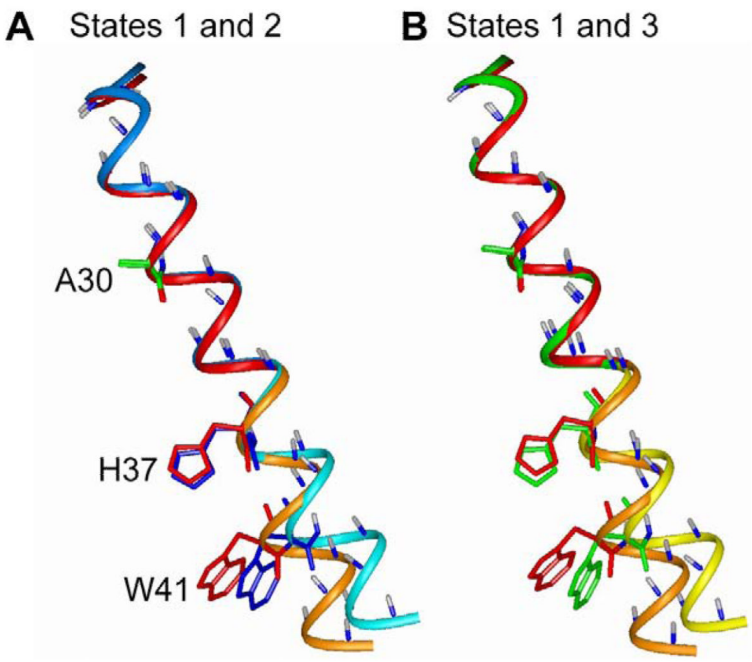

Figure 6.

Comparison of M2TM helical conformations in the three basis states. The helix conformations were constructed using chemical-shift-derived TALOS+ torsion angles (Table 2). **A**. State 1 (red and orange) is favored by amantadine binding and thicker membranes. State 2 (blue and cyan) is promoted by thin membranes and no drug. **B**. State 1 superimposed with state 3 (green and yellow), which is favored by low pH.

Table 1

Isotropic ^{13}C and ^{15}N chemical shifts (ppm) of M2TM residues with significant chemical shift changes among the three conformational states.

Site	State 1 (high pH, thick bilayers, drug binding)			
	V27	S31	G34	H37
N	119.7	121.4	110.4	118.1
CO[a]	178.6	173.1	175.1	175.1
Cα	62.4	61.3	44.9	55.1
Cβ	30.1	59.8	-	30.6
	State 2 (high pH, thin bilayers, apo)			
	V27	S31	G34	H37
N	120.4	114.7	107.1	118.1
CO	177.8	173.7	173.0	175.1
Cα	63.8	61.2	45.7	55.1
Cβ	29.7	60.8	-	27.9
	State 3 (low pH, thick bilayers)			
	V27	S31	G34	H37
N	119.7	114.1	107.8	117.4
CO	177.0	173.7	173.0	174.2
Cα	64.0	61.3	45.7	57.2
Cβ	29.8	61.5	-	26.2

[a] All ^{13}C chemical shifts are referenced to TMS and ^{15}N chemical shifts are referenced to liquid ammonia.

Table 2

M2TM (ϕ, ψ) torsion angles predicted from the SSNMR isotropic chemical shifts using TALOS+ [34].

Residue	Set 1		Set 2		Set 3	
	ϕ	ψ	ϕ	ψ	ϕ	ψ
L26	−64±3	−38±9	−66±2	−38±8	−68±3	−36±9
V27	−67±8	−42±7	−68±9	−39± 13	−66±7	−40±9
V28	*−62±4*	*−45±5*	*−67±11*	*−41±10*	*−63±5*	*−45±9*
A29[b]	*−60±5*	*−43±6*	*−60±5*	*−43±6*	*−60±5*	*−42±8*
A30	−66±4	−39±6	−63±6	−40±7	−64±7	−39±7
S31	−68±8	−40±7	−65±9	−39±6	−66±9	−38±7
I32	−62±5	−41±9	−65±4	−42±9	−64±4	−42±9
I33[b]	*−62±4*	*−38±7*	*−63±3*	*−44±10*	*−64±4*	*−44±9*
G34[c]	**−69±15**	**−37±14**	**−64±4**	**−43±7**	**−65±4**	**−42±7**
I35	−62±5	−44±4	−60±4	−40±5	−63±4	−39±6
L36[c]	**−65±6**	**−26±14**	**−65±7**	**−29±14**	**−62±4**	**−37±9**
H37[c]	**−79±17**	**−31±19**	**−69±7**	**−38±8**	**−64±4**	**−43±5**
L38	−62±5	−36±10	−65±6	−35±9	−65±5	−37±8
I39[a]	−63	−45	−63	−45	−63	−45
L40[a]	−62	−43	−62	−43	−62	−43
W41[a]	−66	−44	−66	−44	−66	−44
I42[a]	−67	−43	−67	−43	−67	−43
L43	−60±3	−40±7	−63±8	−39±7	−63±8	−39±7
Standard deviation	5.1	4.9	2.5	4.0	2.0	2.5

[a] Torsion angles taken from the PDB structure 2KQT [16], which were constrained by N-H bond orientations [36,38] and several distance constraints [61].

[b] Residues whose conformation most approaches the predicted ideal a-helices in hydrophobic environments [57].

[c] Residues exhibiting large conformational changes among different states or large (ϕ, ψ) uncertainties.